NANO LETTERS

Letter

pubs.acs.org/NanoLett

Ultrafast All-Optical Switching with Magnetic Resonances in Nonlinear Dielectric Nanostructures

Maxim R. Shcherbakov,*[,†] Polina P. Vabishchevich,[†] Alexander S. Shorokhov,[†] Katie E. Chong,[‡] Duk-Yong Choi,[§] Isabelle Staude,[‡] Andrey E. Miroshnichenko,[‡] Dragomir N. Neshev,[‡] Andrey A. Fedyanin,[†] and Yuri S. Kivshar*[,‡]

[†]Faculty of Physics, Lomonosov Moscow State University, Moscow 119991, Russia

[‡]Nonlinear Physics Centre and [§]Laser Physics Centre, Research School of Physics and Engineering, The Australian National University, Canberra, ACT 0200, Australia

Supporting Information

ABSTRACT: We demonstrate experimentally ultrafast all-optical switching in subwavelength nonlinear dielectric nanostructures exhibiting localized magnetic Mie resonances. We employ amorphous silicon nanodisks to achieve strong self-modulation of femtosecond pulses with a depth of 60% at picojoule-per-disk pump energies. In the pump–probe measurements, we reveal that switching in the nanodisks can be governed by pulse-limited 65 fs-long two-photon absorption being enhanced by a factor of 80 with respect to the unstructured silicon film. We also show that undesirable free-carrier effects can be suppressed by a proper spectral positioning of the magnetic resonance, making such a structure the fastest all-optical switch operating at the nanoscale.

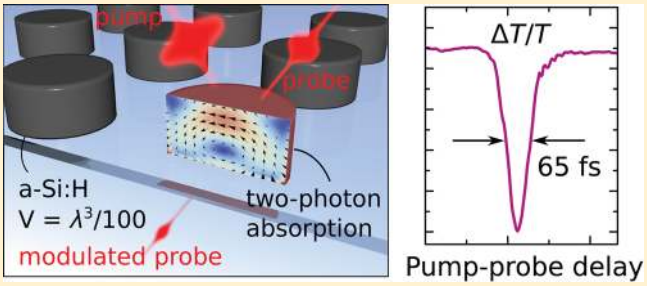

KEYWORDS: *Nonlinear optics, metasurfaces, all-optical switching, silicon photonics, optical magnetism, femtosecond optics*

All-optical signal processing is one of the important directions of photonics aimed toward fast optical communications and high-performance optical computing. Because of the generally weak optical nonlinearities, all-optical Kerr-type effects require macroscopic propagation lengths. On the other hand, in nanophotonics it has been suggested that strong optical field enhancement by means of spatial confinement effects can result in smaller mode sizes and larger modulation depths. Photonic crystals,[1] plasmonic structures,[2,3] metamaterials,[4,5] and micropillar cavities[6] have been employed for ultrafast all-optical switching. However, many of such structures suffer from low efficiency and losses, especially when metallic elements are used for the nanoscale light confinement. On the other hand, high-quality-factor resonators[7,8] have also shown great promise for reducing the energies required for optical switching; however, because the bandwidth of such resonators is narrow their switching speed is limited to nanosecond-scale time frames.

Recently, high-permittivity all-dielectric nanoparticles and nanostructures have emerged as a promising alternative to metallic structures for a wide range of nanophotonic applications. These nanoparticles utilize localized magnetic resonant Mie modes, which were observed experimentally in the entire visible spectral range.[9,10] Nanostructures and metasurfaces fabricated of all-dielectric nanoparticles benefit from both very low intrinsic losses and localized Mie-type modes that make them favorable candidates for improving nonlinearities.[11,12] The study of the third-harmonic generation from silicon nanodisks revealed that the field localization at the magnetic resonance can result in 2 orders of magnitude enhancement of the harmonic intensity with respect to the unstructured bulk silicon.[13,14] Despite the apparent prospects of utilizing all-dielectric Mie-resonant nanostructures for ultrafast all-optical switching, neither pump–probe nor self-action experiments have been reported.

In this Letter, we study experimentally for the first time to our knowledge the ultrafast nonlinear response of all-dielectric nanostructures based on amorphous silicon nanodisks. We demonstrate low-power, 65 fs all-optical switching due to the strong localized magnetic Mie resonances in the subwavelength ($\lambda^3/100$) regime and the pronounced self-modulation of femtosecond (fs) pulses with a depth of 60%. We also demonstrate that undesirable free-carrier effects can be suppressed by a proper spectral positioning of the magnetic resonances, making these dielectric structures the fastest nanoscale all-optical switches so far.

The idea of the proposed nanoscale all-optical switch is presented in Figure 1a. The ultimate goal is to design and fabricate a subwavelength cavity with an ultrafast response, preferably pulse-limited, and a reasonable modulation depth at

Received: July 29, 2015
Revised: September 19, 2015
Published: September 22, 2015

DOI: 10.1021/acs.nanolett.5b02989
Nano Lett. 2015, 15, 6985–6990

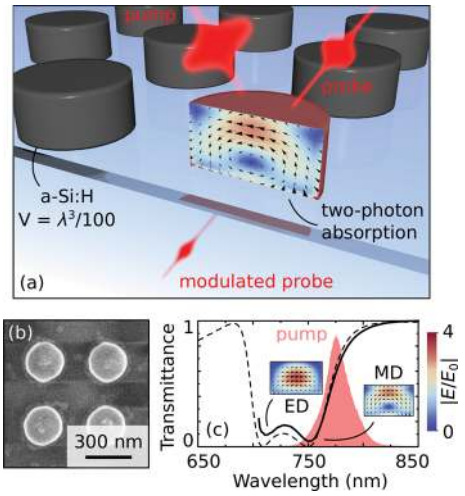

Figure 1. (a) Illustration of ultrafast all-optical switching in resonant silicon nanodisks. (b) A scanning-electron micrograph of one of the samples. (c) Experimental transmittance spectrum of one of the samples (solid curve) measured using the femtosecond pulses (shaded area). Insets show the cross-section local field distributions corresponding to the electric dipolar resonance at 710 nm and magnetic dipolar resonance at 755 nm mapped over the calculated transmittance (dashed curve).

moderate deposited pulse energies. At first, silicon is chosen to be the constituting material; this decision takes advantage of its CMOS technology compatibility, production simplicity, and high refractive index. The latter is a property necessary to gain access to strong Mie-type resonances and in particular to the highly localized magnetic dipolar resonance, which was previously used for the enhanced nonlinear response.[13] Here, we also make use of nanodisks[15,16] instead of other shapes for their two degrees of geometrical freedom and lateral isotropy. In order to fully analyze the effect of optical switching in our nanostructures, one requires two types of experiments: (i) femtosecond pump−probe experiments for determining the lifetimes of the involved transient processes and measuring the switching times and (ii) *z*-scan and *I*-scan experiments for exploring the magnitude of the fs pulse self-modulation. Overall, these experiments will define the applicability of our nanoscale optical switching to applications as pulse limiters, saturable absorbers, and so forth.

Building on the vast knowledge in the field of nonlinear silicon photonics, we fabricate dielectric nanodisks made of hydrogenated amorphous silicon (a-Si:H). a-Si:H is known to exhibit large nonlinearities[17,18] and fast carrier recombination times,[19] which makes it a great nonlinear material. We fabricate arrays of a-Si:H nanodisks using a standard five-step procedure: electron-beam exposure of a negative resist spin coated over a 130 nm a-Si:H film grown by plasma-enhanced chemical vapor deposition, followed by development and reactive ion etching (see Supporting Information, Section I). The radii of the disks are kept in the range of 105−140 nm in order to ensure that the magnetic resonances, having strongly confined optical modes as shown in Figure 1a, overlap with the spectrum of the femtosecond pulses at a central wavelength of about 780 nm used in this study. Figure 1b shows the scanning-electron microscope image of a nanodisk array sample with a radius of r = 125 nm. In the transmission spectrum taken for smaller nanodisks given in Figure 1c, we observe two distinct dips at 710 and 750 nm, which we relate to the eigenmodes of each nanodisk by performing finite-difference time-domain (FDTD) calculations. As seen from the local field maps given in the inset of Figure 1c, the short- and long-wavelength minima of the spectrum correspond to the electric dipolar (ED) and magnetic dipolar (MD) resonances, respectively, which is in good agreement with previous works.[13,16]

In order to explicitly show frequency-degenerate nonlinearities of our nanodisk resonators, we perform regular apertureless *z*-scan[20] and spectroscopic *z*-scan measurements; the results are given in Figure 2a,b, respectively. The data

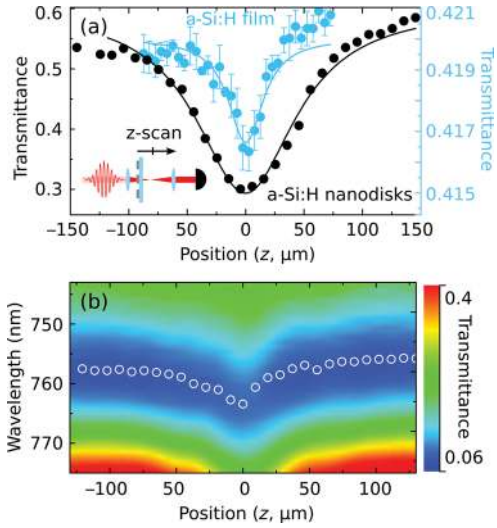

Figure 2. Self-modulation of fs pulses in a-Si:H nanodisk metasurfaces. (a) Experimental *z*-scan trace of the sample (black dots) and its best fit to eq 1 with an effective nonlinear absorption constant of $\beta_{sam} \approx 5.6$ cm/kW (red curve). For the reference, a *z*-scan trace obtained for the initial a-Si:H film is given in light blue with the best fit to eq 1 with $\beta_{film} \approx 0.07$ cm/kW. The inset shows a schematic of the *z*-scan setup used in the experiments. (b) Spectroscopic *z*-scan: sample transmission spectra as a function of *z*. Self-modulation is found to vary from −50% at 775 nm to +21% at 757 nm together with a magnetic resonance shift of 6 nm. Open circles denote the best-fit-based positions of the transmittance minima.

unambiguously demonstrate how light modulates itself when passing through the array of nanodisks, in particular that the transmittance drops by about 60% when the sample is illuminated by a near-resonant focused laser beam. As a consequence, the *z*-scan transmittance strongly depends on the sample position z on the optical axis of the focusing system, as given for a Gaussian pulse[20]

$$T(z) = 1 - \frac{1}{2\sqrt{2}} \frac{\beta_{sam} I L}{1 - \left(\frac{z}{z_0}\right)^2} \quad (1)$$

where β_{sam} is the effective nonlinear absorption constant; I is the estimated focal point intensity of 27 GW/cm^2; L is the sample thickness of 130 nm; z_0 is the focal depth with the best fit value of 52 μm. The focal beam waist is estimated at 2.2 ± 0.5 μm. Using eq 1 we can deduce the effective nonlinear absorption constant to be 5.6 cm/kW, which is almost 2 orders of magnitude larger than that of a bulk a-Si:H film of the same thickness we measure using the same setup, being $\beta_{film} \approx 0.07$ cm/kW. Note that no nonlinear signal was detected from the SiO_2 substrate. Replacing the photodiode with a spectrometer in *z*-scan measurements yields a spectrally dependent trace

DOI: 10.1021/acs.nanolett.5b02989
Nano Lett. 2015, 15, 6985−6990

found in Figure 2b. Applying an intense pulsed field can both increase (+21% at 757 nm) or decrease (−50% at 775 nm) transmission, which is caused by a redshift of the magnetic resonance of $\Delta\lambda = 6$ nm.

Explaining the red shift of the MD resonance requires the analysis of the physics behind the photoinduced processes taking place in the nanodisks. In general, there are three types of nonlinear processes that affect the optical switching: (i) Kerr type processes, including nonlinear refraction and two-photon absorption (TPA). These are the fastest nonlinear processes exhibiting femtosecond characteristic times. (ii) Free-carrier (FC) effects with characteristic times on the picosecond time frame. (iii) Thermal processes, which have the strongest effect, however also the longest (nanosecond) time scale. Speaking of the former contribution, we will see below that the real part of the third-order susceptibility, which corresponds to the Kerr effect, is less pronounced than its imaginary part responsible for TPA. In can also be shown that the observed MD resonance shift cannot be explained by the Kerr refraction alone, as given in the Supporting Information, Section VI. We expect that the TPA process plays a major role in the optical switching because our Ti:sapphire oscillator ($\hbar\omega = 1.6$ eV) is tuned to the band gap-edge regime ($E_g \approx 1.7$ eV in amorphous silicon[19,21]). However, the TPA also induces FCs that are known to affect the refractive index of the a-Si:H, too. The contribution of FC generation to the refractive index of silicon for small Δn is known as[21]

$$\Delta n = -\frac{\omega_p^2}{2n(\omega^2 + \tau_d^{-2})} \tag{2}$$

where τ_d is the Drude damping time, $\omega_p = (4\pi Ne^2/m^*n^2)^{1/2}$ is the FC-induced plasma frequency, N is the photoinduced density of the electron−hole plasma, e is the electron charge, $m^* = 0.12m_0$ is the reduced carrier mass expressed as a fraction of the electron mass m_0, and n is the refractive index of silicon. Here, losses are neglected for the sake of simplicity; for an exact treatment refer to Supporting Information, Section V. For any given N, FC-induced Δn is negative. Upon recombination, the FC relaxation energy is dispersed to the phonon bath. This process heats the sample and leads to slow changes in the refractive index of silicon with a thermo-refractive coefficient of $dn/dT = 4.5 \times 10^{-4}$ K^{-1} as calculated according to ref 19; therefore, FC dissipation leads to a positive Δn. It follows from Mie theory that the spectral position of the magnetic dipolar resonance can be estimated as[9,10,22] $\lambda_0 \sim nd$, where d is a characteristic dimension of the nanoparticle. Taking the positive thermal Δn, negative FC-induced Δn, and small Kerr contributions, we conclude that the red shift present in Figure 2b is mainly due to the sample heating.

In order to distinguish between different self-modulation regimes at different pump powers, we perform I-scan measurements[23] on three different samples with different position of the transmission dip with respect to the spectrum of the pump beam. The results are provided in Figure 3. For the TPA process, transmission is expected to decline linearly with the intensity of the pump beam. For all the three samples, we see that this is the case only up until a certain fluence value. It is important to note that the behavior of $T(I)$ after this critical fluence is different for different samples. Surprisingly, the on-resonance case (red dots and curve) demonstrated the lowest switching depth. The reason for this effect lies in the finite spectral width of the pulses. Indeed, the overall transmittance of

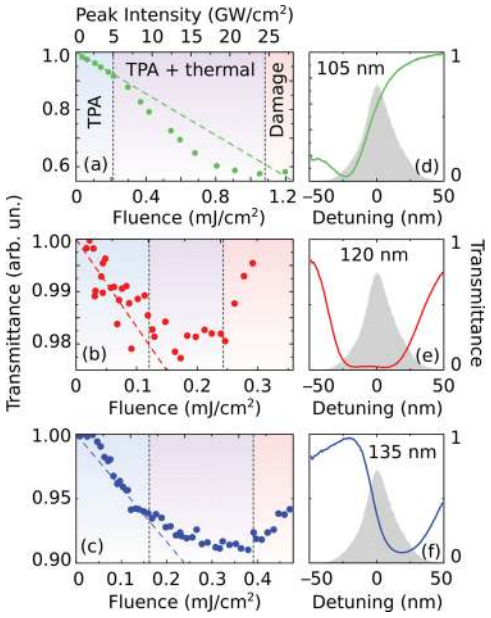

Figure 3. (a−c) Experimental I-scan traces of nanodisk arrays. Three shaded areas in each panel correspond to three different regimes: two-photon absorption (TPA), thermorefractive with TPA, and the one above the irreversible damage threshold. The tilted dashed curves represent linear guides to the eye denoting the TPA-type behavior. (d−f) Corresponding linear transmission spectra (color curves) and the pulse spectrum (gray shaded areas) as a function of detuning from the pulse carrier wavelength. The values of the nanodisks radii are provided.

the pulses consists mostly of the left and right parts of the pulse spectrum as shown in Figure 3e. Those are the less powerful parts of the pulse spectrum, and they do not induce any significant self-modulation.

Microscopically, more peculiar are the cases of the right slope of the resonance shown in Figure 3a and at the left slope of the resonance shown in Figure 3c. Looking at the curves at lower powers, one can conclude that we are indeed addressing the imaginary part of the cubic susceptibility, $\mathrm{Im}[\chi^{(3)}]$, that is, the TPA. If present, the real part of $\chi^{(3)}$ should have manifested itself in blue a red shift of the resonance and ΔT of a different sign for the cases (a,c). Having negative ΔT for both cases grants $\mathrm{Im}[\chi^{(3)}] \gg \mathrm{Re}[\chi^{(3)}]$, which is expected at the resonant near-band gap transitions. Such a strong condition can be found in other resonant nonlinear systems, for example, polymer films.[24] The deviation from the linear law has a different tendency for different slopes due to thermorefraction and the consequent red shift of the MD resonance. We can conclude that up until the irreversible damage occurs at certain fluence values (1, 0.25, and 0.4 mJ/cm^2 for Figure 3a−c, respectively), thermal and TPA contributions may add up both constructively or destructively, depending on the part of the transmittance spectrum considered.

In order to straightforwardly separate the instantaneous TPA process from possible transient FC contributions not seen in static I- and z-scan measurements, a frequency degenerate pump−probe experiment was set up as shown in the inset of Figure 4. We used the same femtosecond laser source with 45 fs pulses (time-bandwidth product ~0.4). After a beam splitter, the pump and probe channels were formed with an intensity proportion of about 25:1. The beams were focused at the sample plane to 30 μm wide spots leading to modest pump

DOI: 10.1021/acs.nanolett.5b02989
Nano Lett. 2015, 15, 6985−6990

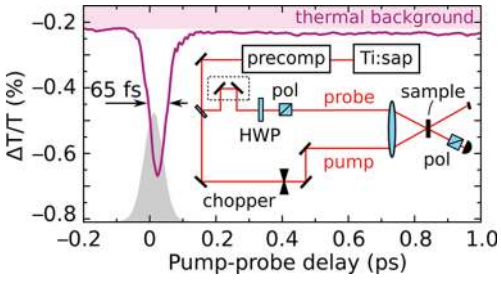

Figure 4. Ultrafast all-optical switching in a-Si:H nanodisks. The purple curve shows the modulation of the probe pulse transmittance as a function of time delay between the probe and pump pulses at low pump powers. An ultrafast, pulse-limited TPA-induced spike is visible as zero delays dominating over the thermal background. Inset: the pump−probe setup used in this study. Precomp is a chirped-mirror pulse precompressor, HWP is a broadband half-wave plate, "pol" are polarizers.

fluences of 30 μJ/cm^2. The horizontally polarized pump beam was modulated by an optical chopper, and the probe beam passed through a delay line. In order to eliminate unwanted scattering of the pump beam to the detector, the probe beam was transformed to be vertically polarized. In addition, a vertically oriented analyzer was added in front of a reversely biased photodiode (see Supporting Information, Section III). The pump-induced modulation ΔT of the probe beam was demodulated using a lock-in amplifier at the chopper frequency.

In an example pump−probe trace in Figure 4, there are two main contributions, the thermal one and the one from the TPA with the latter dominating over the former. The shaded gray area shows the cross-correlation trace as measured by replacing the sample with a beta barium borate crystal and measuring the intensity of the phase-matched sum-frequency beam as a function of the pump−probe delay. The full width at half-maximum (fwhm) of the cross-correlation coincides with the fwhm of the pump−probe trace, and we can infer that the ultrafast contribution to the all-optical switching is an instantaneous two-photon process.

Reaching switching times as low as 65 fs was made possible by the fact that a nanodisk is essentially a low-Q cavity with the Q-factor of the MD resonance of about $Q \approx 15$. The estimated lifetime of a photon inside such a cavity is approximately 40 fs, which is far below the response times of all the conventional silicon-based photonic devices (see a comparative table in the Supporting Information). This lifetime could be the reason for the slight delay of the pump−probe trace with respect to the cross-correlation, as observed in analogous experiments on surface plasmons.[25]

Figure 4 shows no postpump tail in the pump−probe trace that one could expect from the FC relaxation process. Generally, FC effects are considered disadvantageous for all-optical switching in semiconductor-based photonic devices. As long as silicon is concerned, its crystalline form lacks necessary recombination sites, and it may take hundreds of picoseconds for the free-carriers to relax.[26] The situation is better in amorphous silicon; because of the high-order processes, including bimolecular and Auger relaxation, it takes a shorter time for the charges to recombine at larger carrier densities. At critical, subdamage fluences, relaxation times of hundreds of femtoseconds were achieved for FC plasma as dense as 10^{21} cm^{-3}.[21] However, it is not possible to enter the sub-100 fs optical switching regime using FCs, especially at low pump fluences. In order to remove the unwanted FC contribution, we exploit the ability to tailor the dispersion of our metasurfaces and the fact that the FC concentration affects both probe absorption and the MD resonance position. In Figure 5a, we

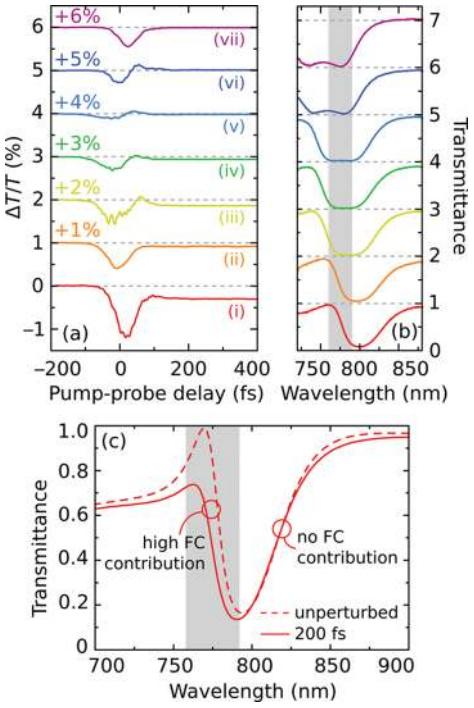

Figure 5. Tailoring the all-optical switching in silicon nanodisks. (a) Pump−probe traces for different samples with corresponding transmittance spectra provided in (b), thermal contribution subtracted. If the pulse spectrum is located at the left slope of the resonance (red curve), a considerable postpulse contribution from free carriers is observed (decay time ∼30 ps). Moving the pulse toward the right slope of the resonance brings the postpulse FC contributions to zero (purple curve). (c) Calculated transmittance spectra of the metasurface in the equilibrium state (dashed curve) and right after the pump pulse has left the medium (solid red curve) at a free carrier density of 5 × 10^{19} cm^{-3}. The shaded areas in (b,c) denote the fwhm of the fs pulses spectrum used for the measurements.

present the pump−probe traces for seven different samples with the thermal contribution removed for better readability; the respective transmittance spectra are given in Figure 5b A strong indication of the FC relaxation could be found at pump−probe delay times $\tau > 150$ fs as given by curves (i)−(iii). The FC relaxation time averages at ∼30 ps, as fitted by the exponential decay law at FC concentration estimated of ∼10^{18} cm^{-3} (see Supporting Information, Section V). This time constant is consistent with the previously reported data[21] for low free-carrier concentrations. However, as the pump and probe beams approach the red-wavelength slope of the resonance, the FC contribution to the pump−probe trace diminishes with respect to the TPA spike for samples represented by (v)−(vii).

In order to demonstrate that exciting Mie-type resonances in the nanodisks can zero FC contributions out, in Figure 5c we provide FDTD transmittance spectra of the nanodisks in two cases. First, the disks are supposed to be at their equilibrium state and silicon is described by our ellipsometry data with n = 3.65 and κ = 0.002 (dashed curve). Second, the nonequilibrium addends to the refractive index from the excited FCs are taken

DOI: 10.1021/acs.nanolett.5b02989
Nano Lett. 2015, 15, 6985−6990

into account ($\Delta n = -0.02$ and $\Delta\kappa = 0.01$, solid red curve) in accordance with the Supporting Information, Section V. Here, n and κ are the real and imaginary parts of the complex refractive index, respectively, and the FC concentration is taken to be 5×10^{19} cm^{-3} for a straightforward illustration of the FC contribution reduction; the value we took is moderate and could be increased by a couple of orders of magnitude before the single-pulse ablation is initiated.[21] One can see from comparing the two cases that, upon FC injection, the transmission curve undergoes both blue shift and reduction. As a consequence, while the leftmost part of the spectrum is considerably affected by FCs, there are wavelength values in the rightmost part for which no changes are detected. Therefore, by tuning the position of the Mie-type resonances in silicon nanodisks with respect to the excitation laser wavelength allows tailoring the FC contributions. In particular, one can zero the FC effects in order to benefit from ultrafast, sub-100 fs TPA-induced nonlinearities.

The silicon nanodisks under study incorporate the advantages of low footprint, ultrafast switching times and low operating power. In our pump−probe experiments, the observed switching of approximately 1% is operated by roughly $E \approx Pd^2/\nu w^2 \approx 13$ fJ per disk. Here, $P \approx 20$ mW is the average pump power detected before the sample, $d \approx 0.22$ μm is the disk diameter, $\nu = 80$ MHz is the repetition rate of the oscillator, and $w \approx 30$ μm is the pump beam-waist diameter. Extrapolating the linear TPA trend to larger fluences, one might expect the complete switching at picojoule-level energies, which is at the level of contemporary Si microring resonators.[7,27,28] The latter, however, have exceedingly larger footprint of 10−1000λ^3 and slower response times of more than 10 ps. Moreover, we can elevate the ultrafast TPA nonlinearity above the thermal contributions by working below the band gap and using heat-dissipating materials like BeO[29] instead of SiO_2. With this in mind, one can consider incorporating these nanocavities into existing CMOS-compatible on-chip silicon photonics circuitry.

One of the biggest advantages of metasurfaces is the ability to spatially vary the parameters of the surface.[30,31] Such spatial variations enable new opportunities for the observed ultrafast switching, namely to construct ultrafast displays that can switch between two or more different images at the femtosecond time scale. Indeed, the differential transmission curves shown in Figure 5 indicate positive or negative modulation values for different times on the scale sub-100 fs. For example, if one constructs a set of pixels using metasurfaces represented by (vi) and (vii), the linear transmission contrast would be low because the samples possess somewhat similar transmittance. On the other hand, it is straightforwardly concluded that a certain degree of contrast could be reached at 50 fs delay due to ΔT having different signs for these samples. Such opportunity remains out of reach for other technologies and might find exciting future applications.

In conclusion, we have demonstrated all-optical switching of fs laser pulses passing through subwavelength ($\lambda^3/100$) silicon nanodisks at their magnetic dipolar resonance. In z-scan experiments, we have observed a modulation of up to 60% and a spectral resonance shift of 6 nm when pumping the nanostructure at picojoule-per-disk powers. We have conducted both I-scan and pump−probe measurements to unambiguously separate the two-photon absorption contributions from the photogenerated free-carrier and thermal contributions. We have shown that the pump-induced modulation of the probe beam is a pulse-limited instantaneous process with the modulation time of 65 fs due to the two-photon absorption. Finally, we have provided a recipe to suppress undesirable contributions from free carriers by tailoring the Mie-type resonance position, thus making such dielectric structures the fastest nanoscale switches reported so far. We believe that our results may be useful for applications in novel on-chip optical limiters, switches and modulators, switchable nanoantennas,[32,33] femtosecond displays, and other nonlinear optical metadevices based on low loss subwavelength dielectric resonant nanoparticles.

■ ASSOCIATED CONTENT

Supporting Information

The Supporting Information is available free of charge on the ACS Publications website at DOI: 10.1021/acs.nanolett.5b02989.

Technical details on the used methods and obtained results. (PDF)

■ AUTHOR INFORMATION

Corresponding Authors

*E-mail: shcherbakov@nanolab.phys.msu.ru.
*E-mail: ysk@internode.on.net.

Notes

The authors declare no competing financial interest.

■ ACKNOWLEDGMENTS

The authors thank R. Oulton, M. Nielsen, and M. Decker for fruitful discussions. The authors acknowledge a financial support from Russian Science Foundation (Grant 14-12-01144, experimental part), Russian Foundation for Basic Research (calculations), and the Australian Research Council.

■ REFERENCES

(1) Mazurenko, D.; Kerst, R.; Dijkhuis, J.; Akimov, A.; Golubev, V.; Kurdyukov, D.; Pevtsov, A.; Sel'kin, A. *Phys. Rev. Lett.* **2003**, *91*, 213903.

(2) MacDonald, K. F.; Sámson, Z. L.; Stockman, M. I.; Zheludev, N. I. *Nat. Photonics* **2009**, *3*, 55−58.

(3) Pohl, M.; Belotelov, V. I.; Akimov, I. A.; Kasture, S.; Vengurlekar, A. S.; Gopal, A. V.; Zvezdin, A. K.; Yakovlev, D. R.; Bayer, M. *Phys. Rev. B: Condens. Matter Mater. Phys.* **2012**, *85*, 081401.

(4) Ren, M.; Jia, B.; Ou, J. Y.; Plum, E.; Zhang, J.; MacDonald, K. F.; Nikolaenko, A. E.; Xu, J.; Gu, M.; Zheludev, N. I. *Adv. Mater.* **2011**, *23*, 5540−5544.

(5) Dani, K. M.; Ku, Z.; Upadhya, P. C.; Prasankumar, R. P.; Brueck, S. R. J.; Taylor, A. J. *Nano Lett.* **2009**, *9*, 3565−3569.

(6) Thyrrestrup, H.; Yüce, E.; Ctistis, G.; Claudon, J.; Vos, W. L.; Gérard, J.-M. *Appl. Phys. Lett.* **2014**, *105*, 111115.

(7) Almeida, V. R.; Barrios, C. A.; Panepucci, R. R.; Lipson, M. *Nature* **2004**, *431*, 1081−1084.

(8) Nozaki, K.; Tanabe, T.; Shinya, A.; Matsuo, S.; Sato, T.; Taniyama, H.; Notomi, M. *Nat. Photonics* **2010**, *4*, 477−483.

(9) Evlyukhin, A. B.; Novikov, S. M.; Zywietz, U.; Eriksen, R. L.; Reinhardt, C.; Bozhevolnyi, S. I.; Chichkov, B. N. *Nano Lett.* **2012**, *12*, 3749−3755.

(10) Kuznetsov, A. I.; Miroshnichenko, A. E.; Fu, Y. H.; Zhang, J.; Luk'yanchuk, B. *Sci. Rep.* **2012**, *2*, 492.

(11) Rose, A.; Huang, D.; Smith, D. R. *Phys. Rev. Lett.* **2013**, *110*, 063901.

(12) Rose, A.; Powell, D. A.; Shadrivov, I. V.; Smith, D. R.; Kivshar, Y. S. *Phys. Rev. B: Condens. Matter Mater. Phys.* **2013**, *88*, 195148.

(13) Shcherbakov, M. R.; Neshev, D. N.; Hopkins, B.; Shorokhov, A. S.; Staude, I.; Melik-gaykazyan, E. V.; Decker, M.; Ezhov, A. A.;

DOI: 10.1021/acs.nanolett.5b02989
Nano Lett. 2015, 15, 6985−6990

Miroshnichenko, A. E.; Brener, I.; Fedyanin, A. A.; Kivshar, Y. S. *Nano Lett.* **2014**, *14*, 6488−6492.
(14) Shcherbakov, M. R.; Shorokhov, A. S.; Neshev, D. N.; Hopkins, B.; Staude, I.; Melik-gaykazyan, E. V.; Ezhov, A. A.; Miroshnichenko, A. E.; Brener, I.; Fedyanin, A. A.; Kivshar, Y. S. *ACS Photonics* **2015**, *2*, 578−582.
(15) Evlyukhin, A. B.; Reinhardt, C.; Chichkov, B. N. *Phys. Rev. B: Condens. Matter Mater. Phys.* **2011**, *84*, 235429.
(16) Staude, I.; Miroshnichenko, A. E.; Decker, M.; Fofang, N. T.; Liu, S.; Gonzales, E.; Dominguez, J.; Luk, T. S.; Neshev, D. N.; Brener, I.; Kivshar, Y. *ACS Nano* **2013**, *7*, 7824−7832.
(17) Ikeda, K.; Shen, Y.; Fainman, Y. *Opt. Express* **2007**, *15*, 17761−17771.
(18) Gai, X.; Choi, D.-Y.; Luther-Davies, B. *Opt. Express* **2014**, *22*, 9948−9958.
(19) Fauchet, P. M.; Hulin, D. *J. Opt. Soc. Am. B* **1989**, *6*, 1024−1029.
(20) Sheik-Bahae, M.; Said, A. A.; Wei, T. H.; Hagan, D. J.; Stryland, E. W. V. *IEEE J. Quantum Electron.* **1990**, *26*, 760−769.
(21) Esser, A.; Seibert, K.; Kurz, H.; Parsons, G. N.; Wang, C.; Davidson, B. N.; Lucovsky, G.; Nemanich, R. J. *Phys. Rev. B: Condens. Matter Mater. Phys.* **1990**, *41*, 2879−2884.
(22) Evlyukhin, A. B.; Reinhardt, C.; Seidel, A.; Luk'yanchuk, B. S.; Chichkov, B. N. *Phys. Rev. B: Condens. Matter Mater. Phys.* **2010**, *82*, 045404.
(23) Taheri, B.; Liu, H.; Jassemnejad, B.; Appling, D.; Powell, R. C.; Song, J. J. *Appl. Phys. Lett.* **1996**, *68*, 1317−1319.
(24) Torruellas, W.; Neher, D.; Zanoni, R.; Stegeman, G.; Kajzar, F.; Leclerc, M. *Chem. Phys. Lett.* **1990**, *175*, 11−16.
(25) Vabishchevich, P. P.; Shcherbakov, M. R.; Bessonov, V. O.; Dolgova, T. V.; Fedyanin, A. A. *JETP Lett.* **2015**, *101*, 787−792.
(26) Doany, F. E.; Grischkowsky, D.; Chi, C. C. *Appl. Phys. Lett.* **1987**, *50*, 460−462.
(27) Wen, Y. H.; Kuzucu, O.; Hou, T.; Lipson, M.; Gaeta, A. L. *Opt. Lett.* **2011**, *36*, 1413−1415.
(28) Martínez, A.; Blasco, J.; Sanchis, P.; Galán, J. V.; García-Rupérez, J.; Jordana, E.; Gautier, P.; Lebour, Y.; Hernández, S.; Guider, R.; Daldosso, N.; Garrido, B.; Fedeli, J. M.; Pavesi, L.; Martí, J. *Nano Lett.* **2010**, *10*, 1506−1511.
(29) Yum, J. H.; Oh, J.; Hudnall, T. W.; Bielawski, C. W.; Bersuker, G.; Banerjee, S. K. *Act. Passive Electron. Compon.* **2012**, *2012*, 359580.
(30) Chong, K. E.; Staude, I.; James, A. R.; Dominguez, J.; Liu, S.; Campione, S.; Subramania, G. S.; Luk, T. S.; Decker, M.; Neshev, D. N.; Brener, I.; Kivshar, Y. S. *Nano Lett.* **2015**, *15*, 5369−5274.
(31) Yu, Y. F.; Zhu, A. Y.; Paniagua-Domínguez, R.; Fu, Y. H.; Luk'yanchuk, B.; Kuznetsov, A. I. *Laser Photon. Rev.* **2015**, *9*, 412−418.
(32) Iyer, P. P.; Butakov, N. A.; Schuller, J. A. *ACS Photonics* **2015**, *2*, 1077−1084.
(33) Makarov, S.; Kudryashov, S.; Mukhin, I.; Mozharov, A.; Milichko, V.; Krasnok, A.; Belov, P. *Nano Lett.* **2015**, *15*, 6187.

DOI: 10.1021/acs.nanolett.5b02989
Nano Lett. 2015, 15, 6985−6990